

Supplementary material

Power-law rheology of adherent cells by local optical stretching and implications for mechanical modelling

Alexander Janik, Tobias Neckernuss, Kay-E. Gottschalk, and Othmar Marti
University of Ulm, Institute for Experimental Physics, Albert-Einstein-Allee 11, 89081 Ulm

S1 Intracellular and cell-to-cell variations of the RI and potential artifacts

Prior to the stretching measurements, the optical path difference of the cell at the measured spot and intracellular location was measured for all cells in regular medium, to estimate the height, and for most cells also in index matched medium. This allows for the calculation of the median height and RI. The results and the calculation procedure can be found in Figure S1 and the caption. The median values are compiled in Table S1.

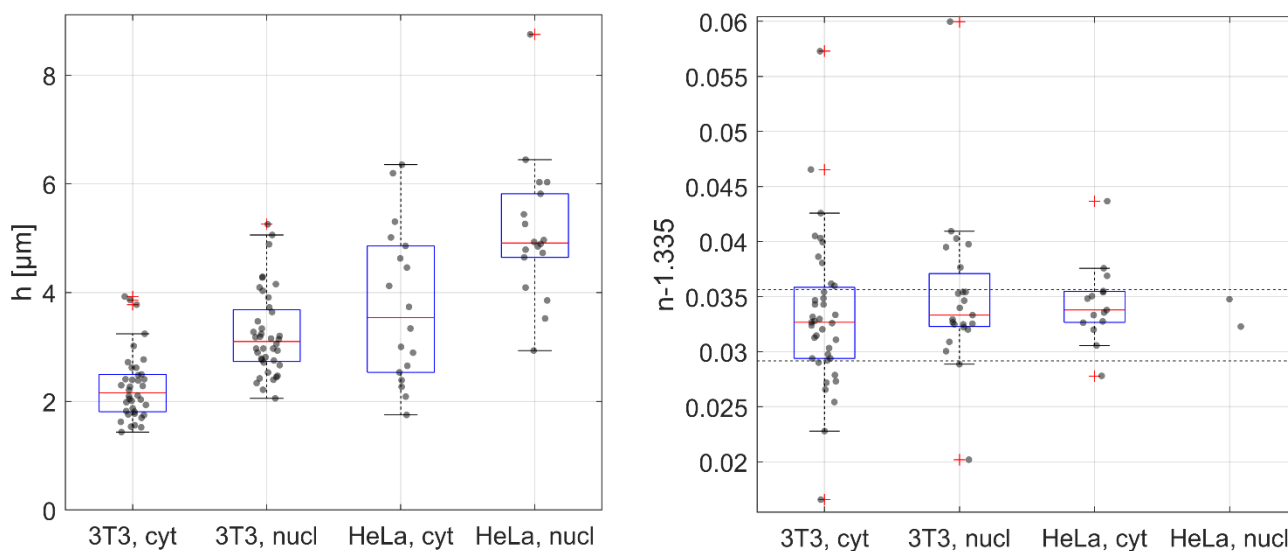


Figure S1 Height and RI distribution for the 3T3 and HeLa cells in Fig. 4 in the main text. The samples were measured both in regular medium ($n_0=1.335$) and index-matched medium ($n=1.3674$). The median phase shift was calculated for both immersion media, which allows the calculation of the median height and RI for each group. **Left:** Height distribution calculated from the measurements in regular medium, under the assumption of a constant refractive index for each group. **Right:** Refractive index distribution calculated from the index matched measurements, assuming that each cell exhibits the previously calculated median height. The dashed lines indicate a $\pm 10\%$ deviation from the refractive index difference compensated by index matching. Regular and index matched measurements were taken from the same samples but from different cells. The phase shift was not determined for all index matched cells since it could not be used for estimation of the height. The height for HeLa cells above the nucleus was estimated assuming the same refractive index difference between nucleus and cytoplasm as in 3T3 cells. Data were acquired from 7 (3) different samples of 3T3 (HeLa) cells.

Table S1: Median cell height and RI with 25th and 75th percentile. Assuming the same height for all cells in turn allows an estimation of the RI distribution from the measured residual phase shift in index matched medium (right). The distributions appear broadened due to the variability of the respective other quantity. The corresponding box plots and a more detailed explanation can be found in Figure S1.

| | 3T3 above cyt. | 3T3 above nucl. | HeLa cyt. | HeLa nucl. |
|---------------------|-----------------------------|-----------------------------|-----------------------------|-----------------------|
| h [μm] | $2.16_{-0.35}^{0.34}$ | $3.10_{-0.37}^{0.59}$ | $3.5_{-1.0}^{1.3}$ | $4.91_{-0.27}^{0.90}$ |
| Δn | $0.0327_{-0.0033}^{0.0032}$ | $0.0333_{-0.0010}^{0.0034}$ | $0.0338_{-0.0011}^{0.0017}$ | |

How do deviations of the RI from $\Delta n = 0.0324$ affect the optical stretcher measurements?

- The median values for different cell lines and measured spots deviate by $\sim 1 - 5\%$ from $\Delta n = 0.0324$. A cell population on a cover slip is measured in normal and subsequently in index matched medium, which differ by $\Delta n = 0.0324$. Therefore, $\Delta n = 0.0324$ is the correct quantity to calculate the Young's modulus according to equation 1 in the main text.
- Local as well as cell-to-cell variations of the RI lead to some variability of the applied force, and thus of the calculated moduli. We however believe this is a minor effect. For the two cell types and intracellular locations, 62% of the measured spots exhibit a RI within $\pm 10\%$ of $\Delta n = 0.0324$ of the index matching medium (see Figure S1). The real spread is smaller, since the RI distribution was calculated assuming the same height for all cells. Furthermore, the variability of the applied force is smaller than the variability of the local measured (projected) RI, since organelles in the cell interior increase the spread of the projected RI, but they do not change the net upward force.
- Some authors have found a lower average RI of the nucleoplasm compared to the cytoplasm in live cells ($\sim 5 - 11\%$ for HeLa [19], $\sim 20\%$ for different eucaryotic cell lines [20]). A lower RI nucleoplasm does however not affect the median elastic modulus. The organelle is slightly compressed during stretching as well as during the index matched reference measurements. The subtraction of the latter eliminates this effect. The fact that the RI of perinuclear cytoplasm and nucleus is similar in our measurements might stem from the fact that we measured in the center of the nucleus, where the nucleoli tend to be.

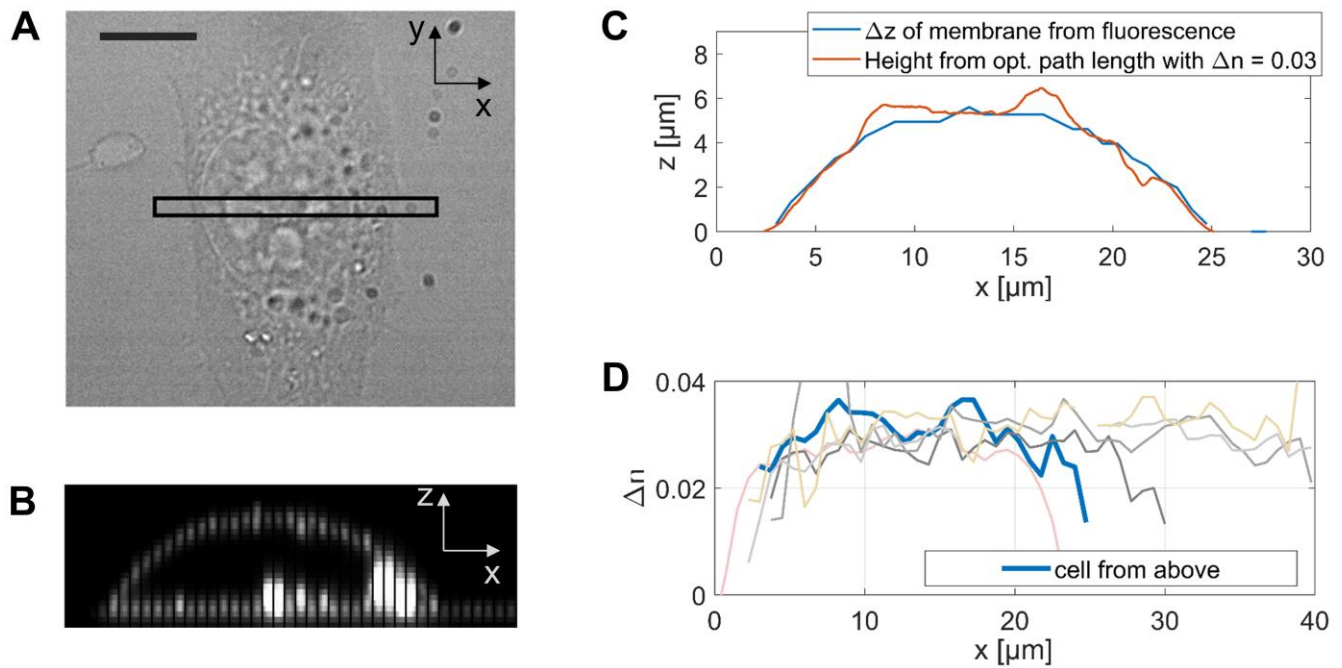


Figure S2 **A**: NIH-3T3 cell. The membrane was stained with CellMask deep red plasma membrane stain (Life Technologies, Darmstadt, Germany) and the detection laser ($\lambda = 633\text{nm}$) was scanned along the indicated area with a high N.A. objective (Zeiss Plan Neofluar, 63x1.3). Scale bar: $10\mu\text{m}$. **B**: Confocal fluorescence x-z cross-section of the cell in A. Fluorescence and interference signal were recorded simultaneously. **C**: The cell height was deduced from the fluorescence cross-section, and is superimposed with the height from the optical path length difference, assuming $n = 0.03$. The optical path length deviates mainly in some spots where objects are discernable in the bright field image in A. **D**: Refractive index cross-sections of six NIH-3T3 cells, deduced from cell height obtained from fluorescence and optical path length difference obtained from interferometric measurement. Near the edge of the cell, the height from fluorescence cannot be reliably determined. The central parts of the cells yield $\Delta n = 0.0302 \pm 0.0028$. The profiles were recorded at room temperature. At $T = 36^\circ\text{C}$, refractive index is seemingly about 10% higher, indicated by the higher concentration of Optiprep necessary for index matching.

S2 Further discussion of potential artifacts

2.1 Surface roughness of HeLa and 3T3 cells and impact by the pericellular brush

Surface roughness might have an impact on the axial force applied by the laser, since a locally tilted membrane would lead to lateral deflection of photons and lower axial force.

Caveoli

A 3T3 cell exhibits $\sim 16 \pm 1$ caveolae and smooth caveolar invaginations [1]. Since their diameter is ~ 70 nm, two caveoli in the area of the stretching beam spot only make up about 0.1% of the surface area.

Tubular extensions

Tubular extensions on the cell surface, such as microvilli, are a prominent feature of different cell lines, and are especially abundant in cancer cells [22]. However, due to their small base dimensions, they do not significantly change the force on the membrane by the $w_0 = 1.61\mu\text{m}$ beam. Their density can be estimated from electron micrographs. Ref. [4] found $r = 50$ nm and a grafting density (ρ_{GD}) of $1.7\mu\text{m}^{-2}$, so the tube bases cover 1.3% of the cell surface. Grafting densities of tubular extensions varied from $0.51\mu\text{m}^{-2}$ to $1.56\mu\text{m}^{-2}$ for HeLa and $0.77\mu\text{m}^{-2}$ to $3.4\mu\text{m}^{-2}$ T47D and TR-75 breast cancer cells [22], which corresponds to surface coverages of 1.3% and 2.7%.

Other surface features

The surface topography of a HeLa cell probed by scanning ion conductance microscopy shows ridges of $\sim 0.5\mu\text{m}$ height and $0.25\mu\text{m}$ width, which make up a small part of the surface area, and relatively flat areas in between [3]. Quantitative AFM studies of surface topography mostly include fixation. A systematic study with paraformaldehyde however found $\sim 3.5\%$ shrinkage and increased roughness from the treatment [6], so it should allow an estimation of the upper bound. A representative AFM line profile of a HeLa cell fixed with glutaraldehyde is shown in [2], digitizing it yields an average tilting angle of the surface of 20.3° [6]. AFM height profiles of paraformaldehyde fixed microglial cells and human primary keratinocytes shown in Ref. [5] largely stay below a tilting angle of 10° . They also examine microroughness of cells by applying high pass filters, isolating features of lateral size below 100nm, and got $R_{RMS} \approx 2$ nm.

These results support our approach of neglecting surface roughness – an assumption has also been made for the established suspended stretcher. It is however possible that there are cell lines or scenarios with a particularly rough topography that impacts the applied force. Extensive blebbing, for instance, has been observed on HeLa cells during cell division [4].

Glycocalyx

This soft layer mainly of polysaccharide chains emerging from the cell membrane can be detected mechanically by AFM indentation. We do however not expect it to impact the signal measured by optical stretching for the following reasons.

1. Since the glycocalyx (GC) has to our knowledge not been observed on 3D RI maps by optical diffraction tomography (ODT), and on our correlated fluorescence- phase shift measurements (Fig. S2), we expect Δn_{GL} to be less than 10% of $\Delta n_{cytoplasm}$. This reduces the force and thus the deformation by at least $10 \times$ and additionally decreases the optical path length difference for a given deformation δ by $10 \times$.
2. The glycocalyx [22][26] and artificial brushes [23] can be described by polymer brush theory, which allows an estimation of mass density, RI and stiffness. Parameters for both hyaluronic acid (HA) biomimetic brushes and cells are compiled in Table S2. We estimate mass density, RI change and relative contribution to the signal from the GC. In summary, the signal contribution is negligible, since brushes are either long and the signal is low due to the low Δn , or Δn is higher, but the layer is flat and stiff. For this we assumed incompressibility and hence material being moved to the stretched center, but no solvent inflow.
3. Chains with high graft density and high RI change are however mostly aligned in parallel (the brush regime [22]). Stretching them would thus mainly lead to medium inflow, i.e. a Poisson's ratio near 0.

This does however not lead to an increase in optical path length measured by our setup, and would thus not disturb the signal.

We also note that the force on the membrane is not lowered for a stiff ($E > 10\text{kPa}$), high RI GC such as the last row of Table S2, since the force on the GC is also transmitted to the Membrane.

Table S2: Estimated parameters for the glycocalyx and impact on optical stretching under the assumption of incompressibility. The cited studies represent the range of parameters found for the GC. The mass concentration in the brush c is estimated from graft density (ρ_{GD}), molecular weight (m_M , assuming 1MDa for the cells from [27] and, for a conservative estimate, 6MDa in [26], based on the higher GC) and height h as $c = \rho_{GD} \cdot m_M/h$. For the cells from references [26][27], we calculate the elastic modulus by $E = 3k_B T \rho_{GD}^{3/2}$. Δn is calculated from the change in refractive index per concentration of the solute dn/dc (0.17 mL/g for hyaluronic acid, similar for most biomolecules [25]). $\Delta n_0 = 0.0327$ is the RI difference at the cell membrane. The deformation of the GC from optical stretching over the deformation of the cell membrane is $\delta_{GL}/\delta_0 = (E_0/E) \cdot \Delta n/\Delta n_0$. It is based on $E_0 = 0.25\text{ kPa}$, the approximate stiffness value obtained for HeLa and 3T3 cells in the main text, and a viscoelastic half-space assumption. $\Delta z_{opt}/\Delta z_{opt,0} = \delta/\delta_0 \times \Delta n/\Delta n_0$ is the relative difference in optical path length, which is the signal measured by the presented setup. The final relative contribution to the signal is $\Delta z_{opt}/\Delta z_{opt,0} \times \delta/\delta_\infty$, which includes a correction factor due to the finite thickness layer: $\delta/\delta_\infty = 1/\left[1 + 0.6719w_0/h + 0.6265\left(\frac{w_0}{h}\right)^2 + 0.04553\left(\frac{w_0}{h}\right)^3 + 0.003623\left(\frac{w_0}{h}\right)^4\right]$ ([15], for indentation with a spherical tip, this correction factor is even smaller [29]). Parameters for the outer brush layer in [26] are difficult to estimate, but due to the low density negligible. In [22], up to 50000 chains per flat cell surface (corresponding to $\rho_{GD} = 10000/\mu\text{m}^2$ including membrane tubes) were directly measured on modified epithelial cells with a dense MUC-1 GC. Some high MUC-1 cancer cells (HeLa, T47D, and ZR-75-1) were found to have comparable grafting densities. With $h = 135\text{nm}$ (contour length: 270nm) and a molecular mass of $m_M = 350\text{kDa}$ we estimate the contribution based on 58 kDa HA brushes, however the layer is most likely stiffer for MUC-1 since m_M is much higher due to the side chains.

| system | height, grafting density, mass concentration in the brush, elastic modulus | $\Delta n/\Delta n_0$ | δ_{GL}/δ_0 | $\Delta z_{opt}/\Delta z_{opt,0}$ | relative signal contribution |
|------------------------------|--|-----------------------|------------------------|-----------------------------------|------------------------------|
| 850 kDa HA brushes [24] | $h=0.43\mu\text{m}, \rho_{GD} = 183/\mu\text{m}^2, c = 0.59\text{ g/L}, E = 40\text{ Pa}$ | 3.0×10^{-3} | 0.019 | 5.6×10^{-5} | 3.6×10^{-6} |
| 58 kDa HA brushes [24] | $h=0.11\mu\text{m}, \rho_{GD} = 9430/\mu\text{m}^2, c = 8.3\text{ g/L}, E = 10\text{ kPa}$ | 0.043 | 0.262 | 0.0011 | 2.4×10^{-6} |
| A549 [27] | $h=0.42\mu\text{m}, \rho_{GD} = 88/\mu\text{m}^2, c = 0.35\text{ g/L}, E=10\text{Pa}$ | 1.8×10^{-3} | 0.046 | 8.2×10^{-5} | 5.1×10^{-6} |
| EA.hy92 [27] | $h = 0.21\mu\text{m}, \rho_{GD} = 251/\mu\text{m}^2, c = 2.0\text{ g/L}, E=48\text{Pa}$ | 0.01 | 0.054 | 5.6×10^{-4} | 7.4×10^{-6} |
| Guinea pig fibroblast [26] | $h=3.4\mu\text{m}, \rho_{GD} = 272/\mu\text{m}^2, c=0.80\text{ g/L}, E=54\text{Pa}$ | 4.1×10^{-3} | 0.019 | 2.6×10^{-6} | 1.76×10^{-6} |
| outer brush layer [26] | $h=37\mu\text{m}, \rho_{GD} = 12/\mu\text{m}^2$ | | | | |
| High MUC-1 cancer cells [22] | $h \sim 0.13\text{nm}, \rho_{GD} \sim 10000/\mu\text{m}^2$ | 0.23 | | E unknown | $\lesssim 10^{-4}$ |

¹ According to Alexander-de Gennes theory, a common brush model to interpret AFM curves [27], the pressure upon deforming a neutral polymer brush of height h by $\varepsilon = \Delta h/h$ is $p = (k_B T/s^3)[(1 - \varepsilon)^{9/4} - (1 - \varepsilon^{3/4})]$ [28]. s is the RMS separation distance of adjacent chains. We calculate $E(\varepsilon) = dp/d\varepsilon$ and perform a Taylor expansion for very small deformations. This gives $E = 3k_B T/s^3$, similar to $E = 13k_B T/(\pi s^3)$ derived for (charged) HA chains in Ref. [24], and we approximate $s = \sqrt{1/\rho_{GD}}$

2.2 Forces due to an electric field gradient

Forces on small dielectric particles in an electric field gradient are exploited in optical traps. For dielectric particles much larger than the wavelength, the resulting forces can be described by ray optics [7], which leads to the interface forces that are the basis of the optical stretcher presented in this paper. Since the laser is not tightly focused in a spot but has a Rayleigh length of $\frac{\pi w_0^2}{\lambda} \approx 13\mu\text{m}$, dielectric particles inside the cell experience a net lateral force pulling them towards the beam center. For a high refractive index object such as a lipid droplet with $n = 1.6$ and $r = 0.25\mu\text{m}$, this results in a maximum gradient force per input power of 10.3 pN/W at a distance of $w_0/2$ (Rayleigh approximation, equation 16 in [8]). This is about 10% of the optical stretching force for $\Delta n = 0.0324$ (108 pN/W). Optical tweezers typically exert much higher forces. A tightly focused laser ($w = w_0/4$) results in an electric field gradient and a resulting lateral force $16\times$ higher for the same power.

Another argument against significant unwanted manipulation of the cell interior is the observation, that the measured phase shift when the laser is on, but stretching is prevented by index matching (intracellular contributions, measured by index matching, Fig. 3) is negative. If small dielectric particle with $n > n_{\text{medium}}$ would be accumulated in the beam due to gradient forces, this would result in a positive phase shift.

2.3 Stretched surface curvature and lensing effect

The cell is deformed by the stretching laser ($2w_0 = 3.22\mu\text{m}$), and the center of the deformed area is probed by a probe beam ($2w_0 = 0.64\mu\text{m}$). Since the probe beam waist is much smaller, a constant phase shift across the beam has been assumed, which is obtained by fitting the interference fringes on the camera (see section 2.3). This assumption and the potential impact of a lensing effect due to the curved, deformed surface, is assessed here.

Silica microspheres of two diameters were used: $1.57 \pm 0.02\ \mu\text{m}$ (Duke Standards, Thermo Fisher Scientific, USA) and $4.5 \pm 0.12\ \mu\text{m}$ (Microparticles GmbH, Germany). Mixtures of water and glycerol were prepared to create a RI difference of $\Delta n \approx 0.0324$ to mimic the locally curved surface of a cell. The RI of the glycerol:water mixtures at $\lambda = 633\text{ nm}$ was estimated as the mean value of [13] (670 nm) and [14] (589 nm). For a glycerol mass concentration $c_m > 0.6$, it is $n = 1.32302 + 0.14827 \cdot c_{\text{mass}}$. First, mixtures with a RI close to $n = 1.4567$ were created (RI of commercial fused silica at 20° and $\lambda = 643.8\text{ nm}$ [12]) to determine the RI of the beads. We obtained $n_{\text{bead}} = 1.4545 \pm 0.0005$ for the $4.5\ \mu\text{m}$ beads and $n_{\text{bead}} = 1.4509 \pm 0.0005$ for the $1.57\ \mu\text{m}$ beads. Then, mixtures of $c_{\text{mass}} = 0.6689$ ($4.5\ \mu\text{m}$, $\Delta n = 0.0323 \pm 0.0005$) and 0.6687 ($1.57\ \mu\text{m}$, $\Delta n = 0.0287 \pm 0.0005$) were prepared. The detection beam spot was positioned in the center on the upper bead surface, and the height difference was measured with the same interferometer used for optical stretching.

The measurement procedure is explained in Figure S3 C and the caption. The obtained diameters are shown in Fig. S3 A.

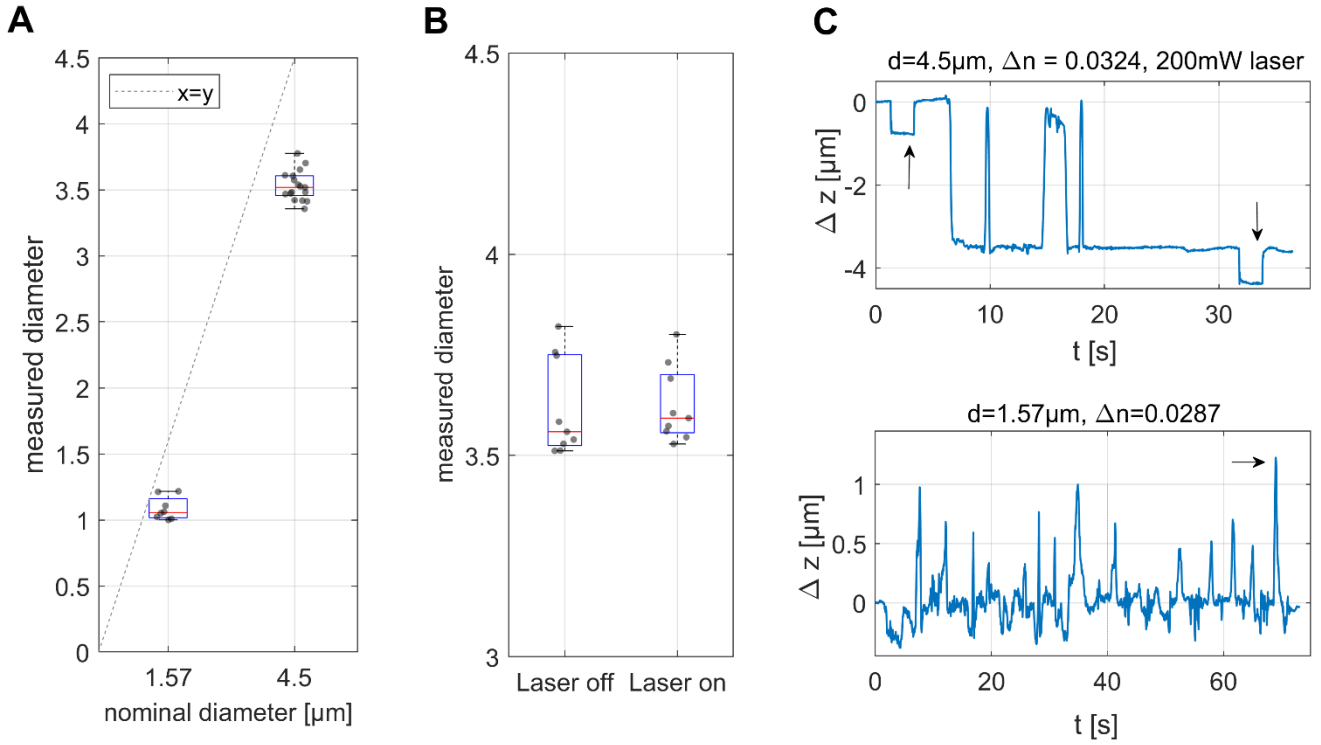


Figure S3 **A**: The bead diameters for both bead sizes ($n=8$ and $n=17$) **B** Bead diameter for $4.5\ \mu\text{m}$ beads with and without the stretching laser **C**: To determine the bead diameter, videos of the interference signal were acquired, while the detection laser spot was moved across the beads. **Top**: $4.5\ \mu\text{m}$ beads. At the beginning, the detection beam is positioned on the bead with the stretching laser at 200mW being applied for two seconds (arrows). **Bottom**: $1.57\ \mu\text{m}$ beads. Some noise due to manually moving the microscope stage can be seen. The bead center is visually hard to see due to low contrast and aberrations, so the highest peak without strong disturbances before and after (arrow) is the measured bead diameter.

The measured diameter exhibits a relative error of 30.6% ($d = 1.57\ \mu\text{m}$) and 21.6% ($d = 4.5\ \mu\text{m}$), while the curvatures are higher by $\times 198/69$ compared to optical stretching lock-in measurements (Fig. 4A) and $\sim \times 12.5/4.3$ compared to the cytochalasin measurements (Fig. 2). For optical stretching, the curvature $\kappa = 1/R$ of the deformed cell surface is estimated from the deformation δ and the $1/e^2$ -beam radius w_0 as illustrated on the right, which leads to $\kappa = \frac{2\delta}{\delta^2 + w_0^2}$. The real shape of the deformation is unknown, but for the extreme case of an elastic half-space, the deformation Δz at a distance w_0 from the center is still about half the maximum deformation δ [15]. Therefore, this geometric estimate of κ appears reasonably conservative. The results and curvatures for beads are compiled in Table S3.

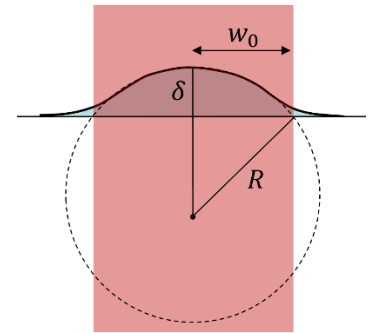


Table S3: The measured bead diameters, absolute errors and curvatures are compared to the deformation (median, 25/75 percentiles) and curvature during lock-in stretching experiments.

| | beads $d = 1.57 \mu\text{m}$ | beads $d = 4.5 \mu\text{m}$ | optical stretching of cells lock-in, 1Hz, HeLa, Fig. 3 |
|---|----------------------------------|----------------------------------|---|
| d_{meas} (mean \pm std) | $1.09 \pm 0.09 \mu\text{m}$ | $3.53 \pm 0.11 \mu\text{m}$ | $\delta = 16.6 \frac{25.1}{13.9} \text{ nm}$ |
| curvature κ | $2 \times 1.27 \mu\text{m}^{-1}$ | $2 \times 0.44 \mu\text{m}^{-1}$ | $\kappa = \frac{2\delta}{\delta^2 + w_0^2} = 0.0128 \mu\text{m}^{-1}$ |
| abs. error over κ : $\frac{d-d_{\text{meas}}}{\kappa}$ | $0.189 \mu\text{m}^2$ | $1.1 \mu\text{m}^2$ | |
| error for $\frac{d-d_{\text{meas}}}{\kappa} =$ $0.189 \mu\text{m}^2$ | | | $\Delta\delta = 0.189 \mu\text{m}^2 \cdot \kappa = 2.4 \text{ nm}$ |

The error of the obtained diameter is apparently comprised of an error scaling with the measured diameter (relative error) and an absolute error. We assume here that the errors scale with the curvature, which is proportional to the refractive power of a lens. Since the curvature of the deformed cell surface is much smaller than the one of the beads, any relative errors become negligible. We now assume the worst case, that the total deviation for the $d = 1.57 \mu\text{m}$ bead ($0.48 \mu\text{m}$) is an absolute error independent of the amount of deformation. Rescaling this value to the curvature of the cell results in an error of 2.4 nm or 14.5% for the lock-in measurements (see last row in Table S3), and 14.2% for the cytochalasin B measurements (Fig. 2). In reality, the error for the cytochalasin experiment might be higher, since the measured deformation appears lower because of the negative phase shift (Fig. 3), which is not corrected for in this measurement. This does however not change any interpretations as this is more of a qualitative measurement. Since the RI difference of the $d = 1.57 \mu\text{m}$ bead was $\Delta n = 0.0287$ instead of $\Delta n = 0.0324$, we conclude that the optical stretcher slightly overestimates the elastic modulus by less than 16%.

Another potential artifact is a thermal lensing effect resulting from heating and a RI gradient above the cell. If this causes an error proportional to the deformation, this would not correctly be taken into account by subtracting the reference measurement. To see whether the presence of a thermal gradient affects the measured height, Δz was measured with the laser on at a power of 200 mW with the waist on the upper surface of the bead (Fig. S3 C, first arrow). In analogy to stretching, a reference measurement is taken at a nearby spot without a bead, and subtracted (Fig. S3 C, second arrow). The results are shown in Figure S3 B and are compiled in the following table. The measured height difference deviates by only 0.3% and can thus be neglected.

| | Laser off | Laser on |
|---|---|--|
| Δz for $n - n_{\text{medium}} = 0.0324$ | $\Delta z_{\text{off}} = 3.62 \pm 0.12$ | $\Delta z_{\text{on}} = 3.63 \pm 0.09$ |

S3 E_0 - β correlation for individual 3T3 and HeLa cells

In Figure 5 in the main text, the medians are fitted, but to examine if our measurements exhibit a correlation between $\ln E_0$ and β , we additionally fitted the $E^*(\omega)$ -curves of individual cells. We observed, that individual noisy data points at a single frequency lead to large errors in the resulting fit. Therefore we performed robust fits minimizing the sum of absolute errors. We also included the periphery (Fig. S5) since it exhibits a clear E_0 - β correlation.

There seems to be a weak correlation for nucleus and cytoplasm in Figure S4 A and a stronger one for the periphery. Despite the robust fit there are a few erroneous data points at $\beta = 0$. We decided not to exclude them, and averaging over nucleus and cytoplasm exhibits almost no negative correlation between individual cells ($R^2 = 0.035$, Fig. S4 B). One factor that reduces the accuracy for individual cells is the fact that for calculation of E^* , several cells of the same sample are later measured in an index-matched medium,

and the median of these measurements is subtracted from the value obtained from stretching the individual cell. Since we want to correct an intracellular contribution to the signal, we can expect that it is proportional to the height of the measured cell. After weighting the signal from RI matched cells with the height of the individual cell before subtraction, a weak correlation of E_0 and β becomes apparent ($R^2 = 0.15$, Fig. S4 C). For calculation of the medians in the main text, this only has a minor effect. In Figure S4 D we did not incorporate this, but we averaged over nucleus, cytoplasm and periphery of each cell. A stronger correlation can be seen.

Hecht et al. [17] found E_0 positively and β negatively correlated with the local height of the cell for $h < 0.5 \mu\text{m}$, which might indicate, that a negative E_0 - β correlation is actually an effect of the underlying stiff substrate. It is frequently claimed that this effect is negligible for indentation depths $<10\%$ of the local height, but the stress profile in an elastic continuum heavily depends on the lateral size of the deformed area [15]. So in Fig. S4 E, E_0 and β are plotted over the local height. Below $h = 0.8 \mu\text{m}$, where the substrate effect should become more and more pronounced, there is no correlation. An uncertainty of the height measurement is most likely not the reason for the absence of correlation, as we expect it accurate up to $\pm 0.05 \mu\text{m}$ for such small heights. The fact that the median β is very similar to the other intracellular locations also suggests that the E_0 - β correlation is not due to the stiff substrate. Park et al. [21] observed on patterned substrates and human airway smooth muscle cells, that the stiffness E_0 increased and β decreased in corners with focal adhesions and stress fibers, but not near straight cell edges. For NIH-3T3 cells, this could explain the E_0 - β correlation, since the periphery spots were mostly in such areas, while for HeLa cells, there were also areas resembling lamellipodia.

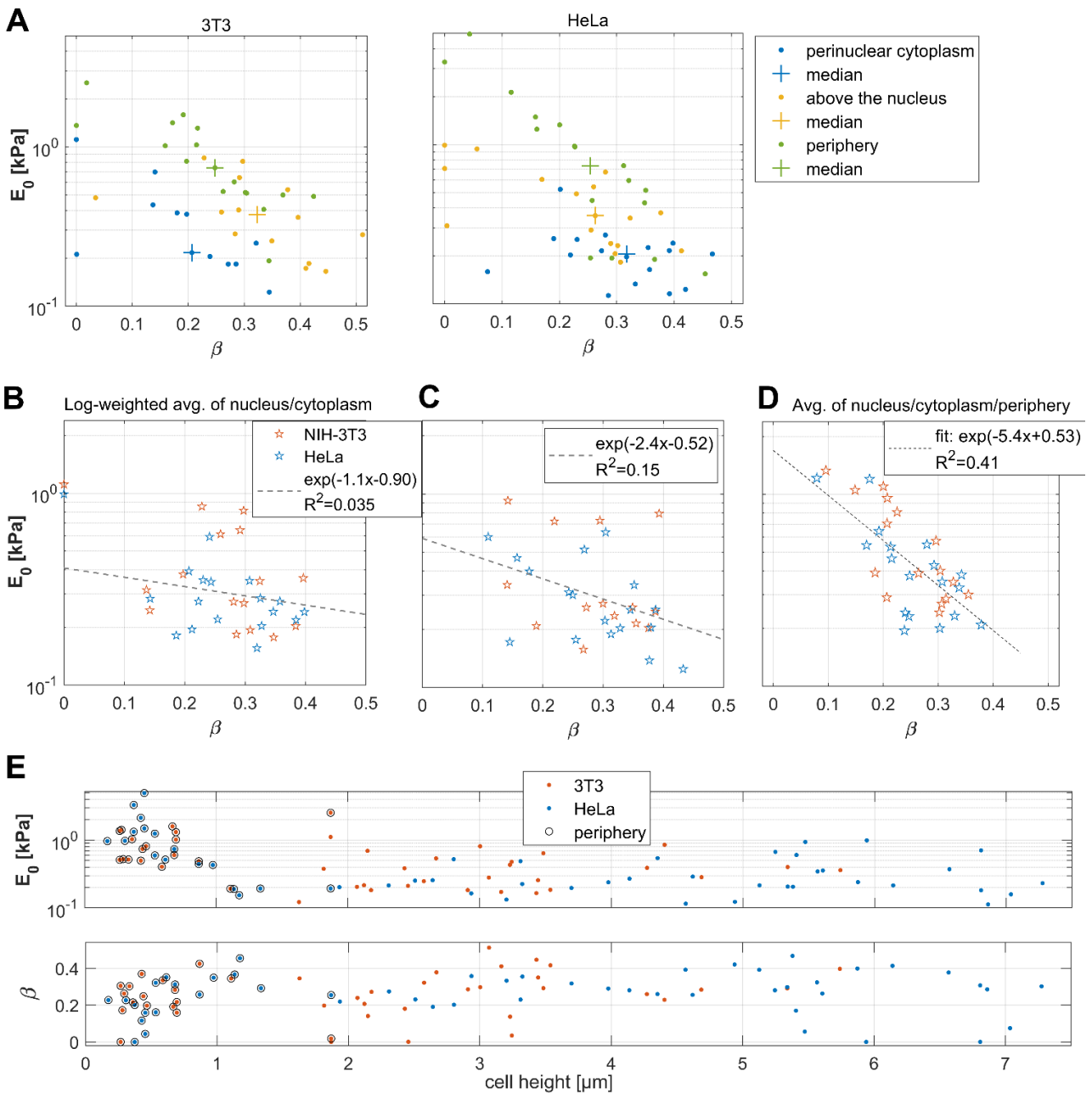


Figure S4 Correlation of E_0 and β between individual cells. **A:** $E^*(\omega)$ was fitted with the structural damping equation (eq. 9, main text) for each cell and intracellular location. Since single outliers especially at $\omega = 1\text{Hz}$ but also at $\omega = 480\text{Hz}$ strongly impact the fitting result, robust fitting was used and the sum of absolute errors was minimized. Data are the same as in Figure 5, but the periphery (Figure S5) is additionally included. **B:** The data from **A**, with above nucleus and cytoplasm log-weighted averaged for each cell. **C:** To improve the accuracy for individual cells, the index-matched measurement to be subtracted, which estimates the intracellular negative phase shift, was weighted with the measured height for each cell. **D:** Log-weighted average of above nucleus, cytoplasm and periphery. **E:** To examine a potential effect of the stiff substrate on the measurements in the periphery, E_0 and β are plotted over the local cell height.

We found three publications that examined cell-to-cell $\ln E_0$ - β correlations for MEFs or 3T3 cells (Table S4). The slope $\ln \tau_0 \approx -5.4$ is lower than for Cai et al.[18] and much lower compared to the other two and to the $\ln E_0$ - β correlation for MEF/3T3 between different AFM studies in the main text (Fig. 5D). Cai et al. indented with much larger tips and contact area ($13.4\mu\text{m}^2$), which is more similar to optical stretching. Also their data were much noisier. A plausible explanation for the low slope and the broad distribution for optical stretching is, that there is some noise in β , which makes the fit fail to capture the steep slope. It should be noted that most publications that examine the E_0 - β correlation do so between samples with different drug treatments or cell lines, but rarely for individual cells.

Table S4: Results from fitting $\ln E_0$ over β in Fig. S4, and comparison with publications that examined the $\ln E_0$ - β correlation for populations of mouse embryonic fibroblasts (MEFs) or NIH-3T3 cells with AFM [16][17][18]. Results from [18] have been digitized using [6].

| | $\ln(\tau_0[\text{s}])$ | $\ln(1/j_0[\text{kPa}])$ |
|---|-------------------------|--------------------------|
| Fig. S4 (HeLa/NIH-3T3) | -2.4/-5.4 | -0.52/+0.53 |
| Hecht et al. (MEF) [16] | -27.2 | 6.4 |
| Schierbaum et al. (MEF) [17] | -26.0 | 3.0 |
| Meta analysis of 3T3 and MEF AFM studies (main text Fig. 5D) | -26.6 | 5.6 |
| Cai et al (NIH-3T3) [18] | -9.4 | 7.9 |

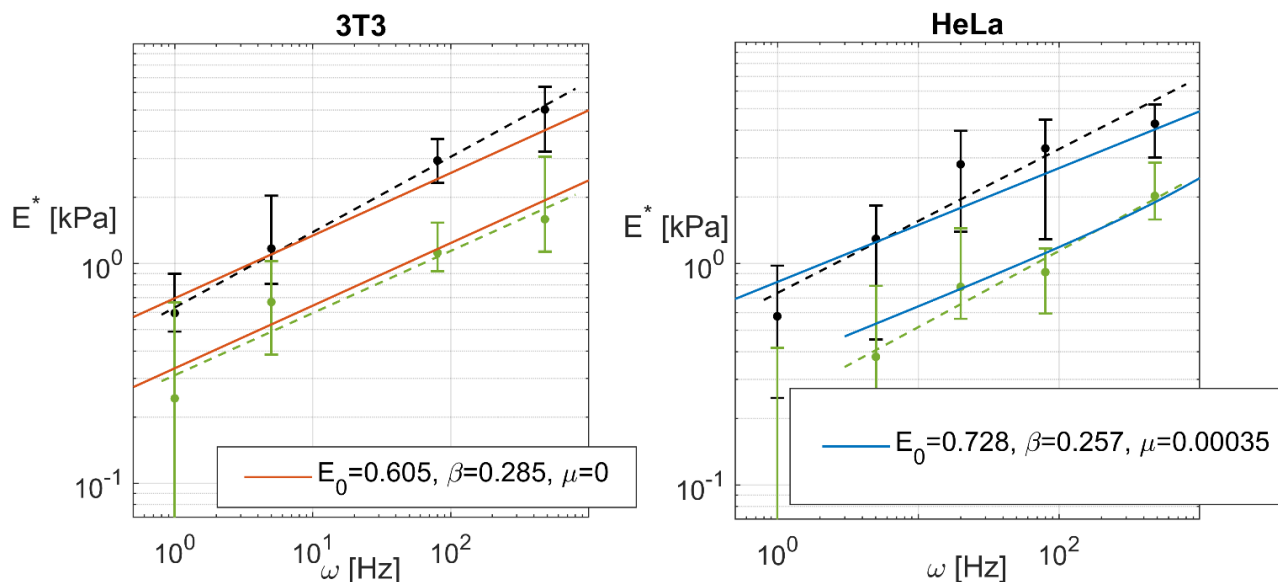


Figure S5: The fits of the median values in the periphery for both cell types have been added for completeness. They were conducted on the same cells as in Figure 5, main text, and measurement and evaluation are analogous to those data for nucleus and cytoplasm. Spots were chosen close to, but not right next to the edge of the cell, where much fewer intracellular structures were visible than in the cell center. Median cell heights at the measurement spots: 3T3: $0.44\mu\text{m}$, HeLa: $0.55\mu\text{m}$. The data point for $1\text{Hz}/E''/\text{HeLa}$ has been excluded from the fit. The reason for the low value is that the 1Hz measurements are noisy and the deformations in the periphery are low, and if the real or imaginary part of the deformation for a cell is negative it is set to zero.

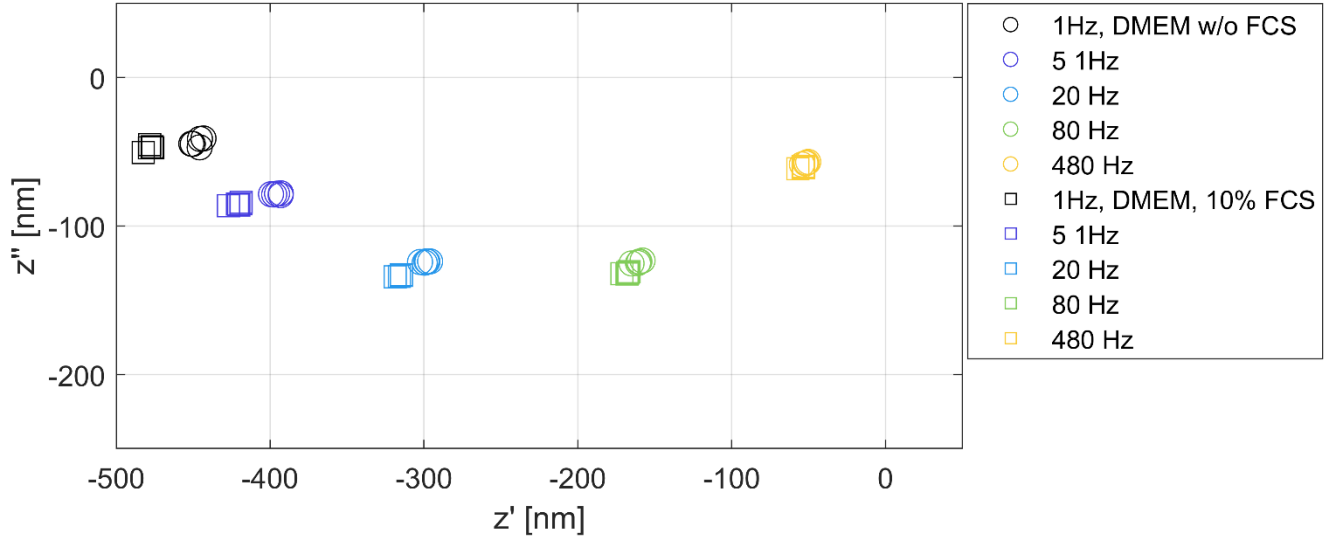


Figure S6: Multiple measurements in two different media without cells at $P_{sample,mean} = 315\text{mW}$. z' and z'' is the apparent deformation, an artifact, that results from a phase shift due to heating of the water column by the laser (see Figure 1 F in the main text, here: peak-to-peak app. deformation). DMEM with 4.5gL^{-1} glucose, 5.958gL^{-1} pH buffer and no phenol red is compared to the same medium with 10% FCS. The relative error is similar for the five frequencies. Without FCS (with FCS), it is on average $\frac{STD(z')}{|z'|} = 1.21\%$ (1.07%) and $\frac{STD(z'')}{|z''|} = 1.53\%$ (1.27%). While the artifact is higher with FCS in absolute terms, its relative (and also absolute) variability is lower. The artifact is subtracted by a reference measurement next to the cell, so we conclude that FCS can be added without a significant deterioration of the signal-to-noise ratio for lock-in measurements.

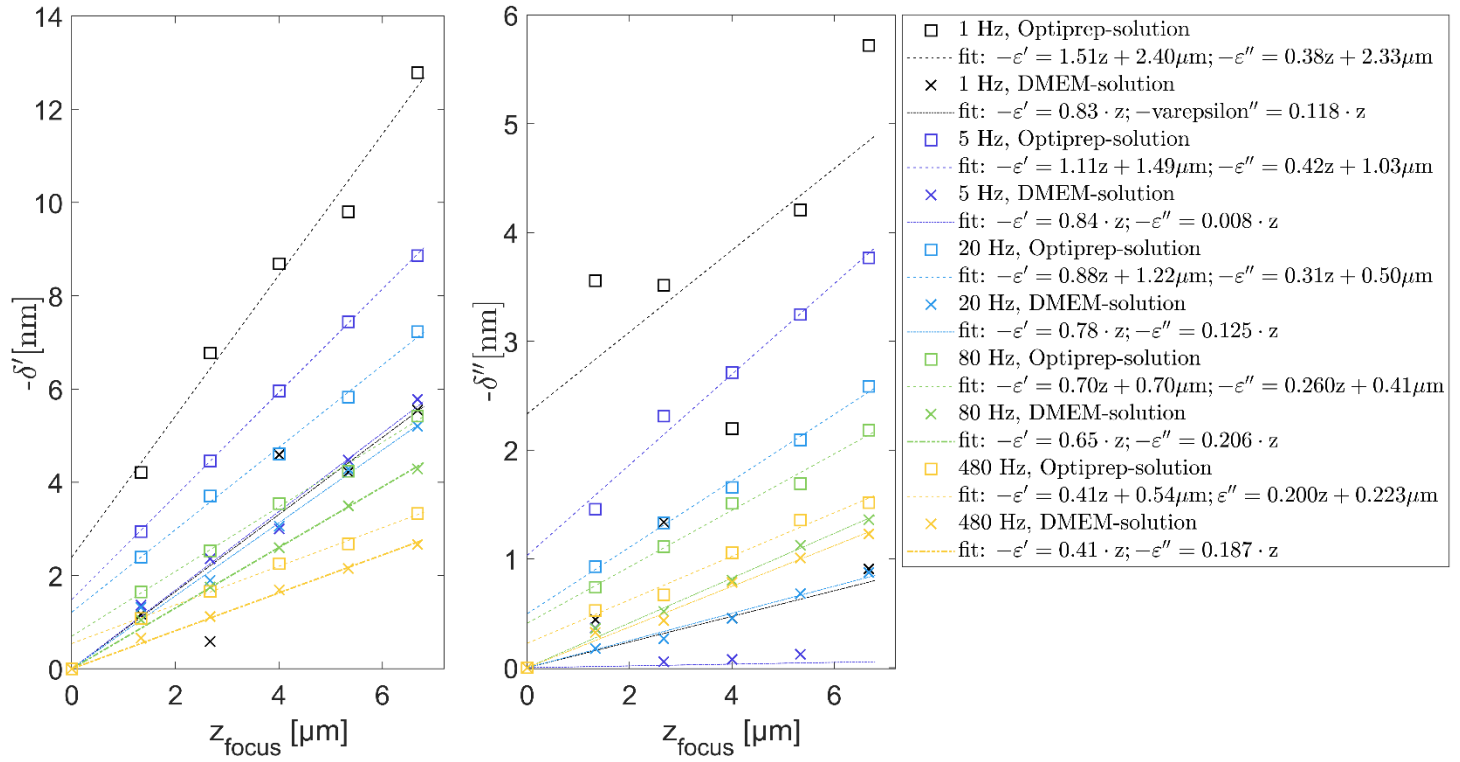


Figure S7: Apparent in-phase and out-of-phase deformation when changing the focal height at $P_{\text{mean,sample}} = 63\text{mW}$ [15]. The minus sign reflects the negative phase shift from heating of the medium. While the phase shifts from water are proportional to the focal height, there appears to be a jump for optiprep within the first 1.33 microns, which is however below the focal height when we measure cells in the perinuclear cytoplasm or above the nucleus.

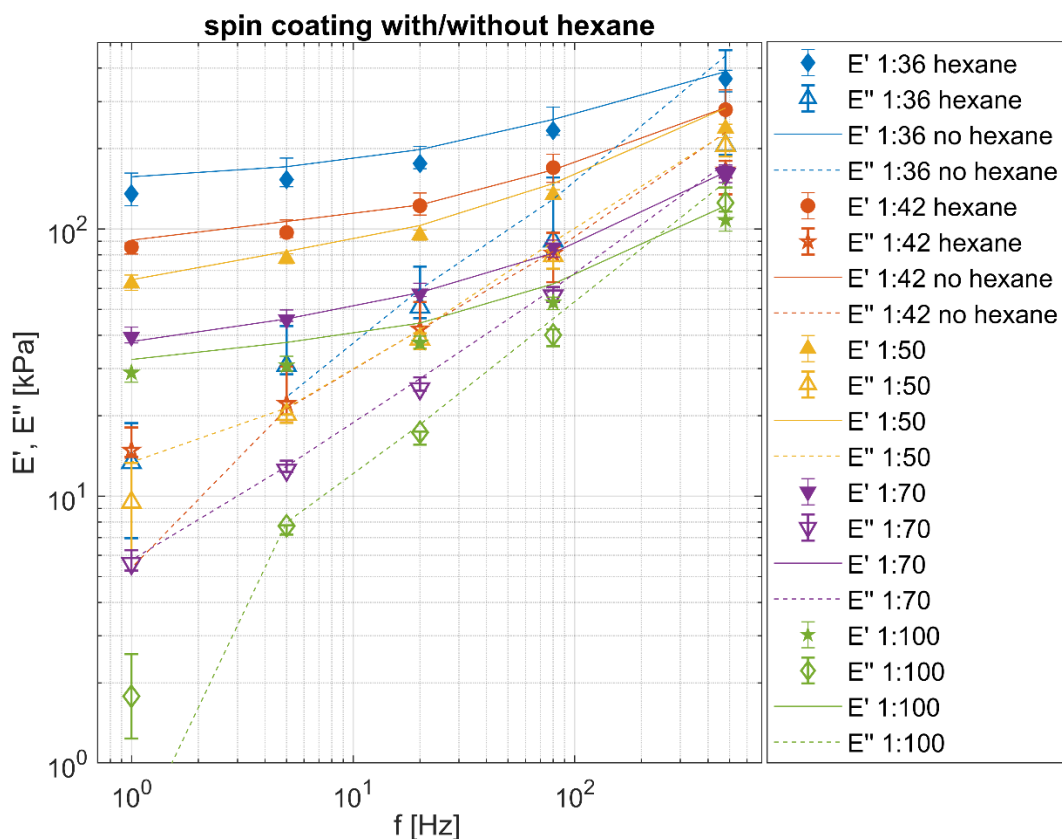


Figure S8 Optical stretching of PDMS thin films in air. Comparison of median complex modulus from $\sim 10 \mu\text{m}$ films spin coated at 7000 rpm (filled and open symbols) vs. $\sim 10 \mu\text{m}$ films spin coated at 280 rpm, where PDMS mixture was dissolved in $5 \times$ the amount n-hexane (solid and dashed lines, 1:5 per weight). N-hexane: n=2/2/2/1/1 films measured for 1:36/42/50/70/100; No hexane: n=2/2/3/2/2. A systematic deviation is only present for the 1:100 film presumably because only one sample was measured. Error bars are 25/75 percentiles and are only shown for hexane samples for clarity.

References

- 1 P. U. Le, G. Guay, Y. Altschuler and Ivan R. Nabi, *J. Biol. Chem*, 2002, **277**, 3371–3379.
- 2 K. S. Kim, C. H. Cho, E. K. Park, M.-H. Jung, K.-S. Yoon and H.-K. Park, *PLoS One*, 2012, **7**, e30066.
- 3 J. Adler, A. I. Shevchuk, P. Novak, Y. E. Korchev and I. Parmryd, *Nat. Methods*, 2010, **7**, 170–171.
- 4 K. R. Porter, V. Fonte and G. Weiss, *Cancer Res.*, 1974, **34**, 1385-1394.
- 5 P. D. Antonio, M. Lasalvia, G. Perna and V. Capozzi, *Biochim. Biophys. Acta*, 2012, **1818**, 3141-3148.
- 6 S. O. Kim, J. Kim, T. Okajima and N.-J. Cho, *Nano Conver.*, 2017, **4** (5).
- 7 P. Polimeno, A. Magazzù M.A. Iati, F. Patti, R. Saija, C. Boschi, M.G. Donato, P.G. Gucciardi, P.H. Jones, G. Volpe and O.M. Maragò, *J. Quant. Spectrosc. Radiat. Transf.*, 2018, **218**, 131–150.
- 8 Y. Harada and T. Asakura, *Opt. Commun.*, 1996, **124**, 529–541.
- 9 Abbate, G. and Bernini, U. and Ragozzino, E. and Somma, F., *J. Phys. D: Appl. Phys.*, 1978, **11**, 1167.
- 10 M. Wolff, J.J. Mittag, T.W. Herling, E. De Genst and C. M. Dobson, T.P.J. Knowles, D. Braun and Buell, A.K., *Sci. Rep.*, 2016, **6**, 22829.
- 11 R. Piazza, *Soft Matter*, 2008, **4**, 1740-1744.
- 12 R. M. Waxler and G. W. Cleek, *J. Res. Natl. Inst. Stand. Technol.*, 1971, **75A**, 279–281.
- 13 R. Bochert, A. Zhivov, R. Kraak, J. Stave and R.F. Guthoff, *Br. J. Ophthalmol.*, 2005, **89**, 1351–1355.
- 14 C. S. Miner, and N.N. Dalton, *Glycerol*, American chemical society monograph series, 1953.
- 15 A. Janik, *PhD thesis*, Ulm University, 2024
- 16 F. M. Hecht, J. Rheinlaender, N. Schierbaum, W.H. Goldmann, B. Fabry, and T.E. Schäffer, *Soft Matter*, 2015, **11**, 4584–4591.
- 17 N. Schierbaum, J. Rheinlaender and T. E. Schäffer, *Soft Matter*, 2019, **15**, 1721–1729.
- 18 P. Cai, Y. Mizutani, M. Tsuchiya, J.M. Maloney, B. Fabry, K. J. Van Vliet and T. Okajima, *Biophys. J.*, 2013, **105**, 1093–1102.
- 19 K. Kim and J. Guck, *Biophys. J.*, 2020, **119**, 1946–1957.
- 20 A. Biswas, O. Muñoz, K. Kim, C. Hoege, B. M. Lorton, D. Shechter, J. Guck, V. Zaburdaev and S. Reber, conserved nucleocytoplasmic density homeostasis drives cellular organization across eukaryotes, *bioRxiv preprint*, 2023.
- 21 C. Y. Park, D. Tambe, A. M. Alencar, X. Trepatt, E. H. Zhou, E. Millet, J. P. Butler and J. J. Fredberg, *Am. J. Physiol. Cell Physiol.*, 2010, **298**, C1245–C1252.
- 22 C. R. Shurer, J. C.-H. Kuo, L M. Roberts, G. W. Feigensohn, H. L. Reesink and M. J. Paszek, *Cell*, 2019, **177**, 1757–1770.
- 23 S. Attili, O. V. Borisov and R. P. Richter, *Biomacromolecules*, 2012, **13**, 1466-1477.
- 24 H. Davies-Strickleton, N. S. Baranova, N. El Amri, L. Coche-Guérente, C. Verdier, L. Bureau, R. P. Richter and D. Débarre, *Mat. Biol.*, 2019, **78-79**, 47-59.
- 25 A. Theisen, C. Johann, M. P. Deacon, S. E. Harding, *Refractive Increment Data-Book for Polymer and Biomolecular Scientists*, Nottingham University Press, 2000.
- 26 M. Dokukin, Y. Ablavaeva, V. Kalaparathi, A. Seluanov, V. Gorbunova and Igor Sokolov, *Biophys. J.*, 2016, **111**, 236–246.
- 27 M. Targosz-Korecka, K. E. Malek-Zietek, D. Kloska, Z. Rajfur, E. Ł. Stepien, A. Grochot-Przeczek and M. Szymonski, *Biochim. Biophys. Acta*, 2020, **1864**, 129533.
- 28 I. Argatov, F. M. Borodich and Xiaoqing Jin, *Front. Mech. Eng.*, 2022, **8**, 931271.
- 29 E. K. Dimitriadis, F. Horkay, J. Maresca, B. Kachar and R. S. Chadwick, *Biophys. J.*, 2002, **82**, 2798-2810.